A biophysical study of the interactions of palladium(II), platinum(II) and gold(III) complexes of aminopyridyl-2,2'-bipyridine ligands with RNAs and other nucleic acid structures

Francesca Binacchi,[a] Cassandra Elia,[a] Damiano Cirri,[a] Corjan van de Griend,[c] Xue-Quan Zhou,[c] Luigi Messori,[b] Sylvestre Bonnet,[c] Alessandro Pratesi,[a] Tarita Biver[a]*

Abstract

Metal compounds form an attractive class of ligands for a variety of nucleic acids. Five metal complexes bearing aminopyridyl-2,2'-bipyridine tetra dentate ligands and possessing a quasi-planar geometry were challenged toward different types of nucleic acid molecules including RNA polynucleotides in duplex or triplex form, an RNA Holliday four-way junction, natural double helix DNA and DNA G-quadruplex. The binding process was monitored comparatively using different spectroscopic and melting methods. The binding preferences that emerge from our analysis are discussed in relation to the structural features of the metal complexes.

1 Introduction

Beyond the cornerstone anticancer metal complex cisplatin,[1] some research groups focus now their attention on other coinage metal centers.[2] Au(III) and Pd(II) have similar coordination but different chemical properties, which may result in different biological activities. The choice of the ligand plays a major role: for Au(III) to limit the tendency to be reduced to Au(I) or Au(0) in biological media,[3,4] for Pd(II) to restrict the greater kinetic lability. In this work, we focus more on Pd(II) complexes, but within a set of metal complexes which also contains the Pt(II) and Au(III) counterparts for comparison purposes. A study carried out on palladium complexes with heterocyclic carbenes, which were compared to gold and silver analogues, revealed that cytotoxicity increases with the electron donor properties of substituents on the polypyridyl ligands.[5] As for the ligands, we selected tetradentate nitrogen ligands, as they were found to form stable Pd(II) complexes, with improved ability to reach their biological target.[6, 7] Pd(II) complexes with similar ligands are already known to have interesting properties and, in some cases, showed stronger anticancer activity compared with their Pt(II) analogues. For instance, Pd(II) and Pt(II) analogues with quinoline and morpholine ligands revealed that Pd(II) complexes were more effective as anticancer agents, and also acted as antibacterial agents.[8] Pd(II) coordinated by two cis chloride ligands and a bidentate ligand was found to cross the cell membrane interact with DNA and or with proteins in the cytoplasm.[9] Overall, Pd(II) complexes have chemical characteristics and properties similar to (or even better than) those of Pt(II) complexes, with a mechanism of action as anticancer drugs that is often related to their ability to interact with DNA (even if not exclusively) via binding modes that are mainly non-covalent, among which intercalation plays the main role. This is the case of Pd(II) bipyridine,[10, 11] Pd(II) phenyl-imidazole [6] or binuclear Pd(II)-benzothiazole complexes.[12] Thiosemicarbazones, as well as phosphines, were used for the synthesis of Pd(II)-containing metal compounds having simultaneously anti-tumor, anti-bacterial, anti-microbial, and antioxidant effects; their cytotoxicity was ascribed, also in this case, to DNA intercalation.[13] A better π-π interaction plays a role also in the case of the possible binding to G-quadruplex (G4) tetrads. In this frame, tridentate terpyridine ligands were found to favour G4 stabilisation and Pd(II) ones have the better π-π stacking respect to Cu(II) and Pt(II) species.[14]

Despite the efforts of the scientific community to unravel the activity of many metal complexes to be used as drugs, there is still room for mechanistic studies on solution equilibria, which may both enlighten the potential medicinal interest of a new

[a] *University of Pisa, Department of Chemistry and Industrial Chemistry, Via G. Moruzzi 13, 56124 Pisa, Italy. Corresponding author T.B. tarita.biver@unipi.it*
[b] *Laboratory of Metals in Medicine (MetMed), Department of Chemistry "Ugo Schiff", University of Florence, Via della Lastruccia 3-13, 50019 Sesto Fiorentino, Italy.*
[c] *Leiden Institute of Chemistry, Leiden University, 2333CC Leiden, The Netherlands.*
† Footnotes relating to the title and/or authors should appear here.
Electronic Supplementary Information (ESI) available: [details of any supplementary information available should be included here]. See DOI: 10.1039/x0xx00000x

complex and help to define robust structure/reactivity relationships. This is particularly true for DNA-binding studies, where the role of non-canonical structures (G4, i-motifs) stabilisers has been evidenced.[15-17] This is even more true for RNA studies that are less abundant, compared with DNA, and which may concern both polynucleotides or oligomers forming peculiar structures (as the Holliday four-way junction considered in this work). Mechanistic solution studies on the interaction between Pd(II) complexes and poly/oligo RNAs are quite rare[18-20] whilst, to the best of our knowledge, RNA four-way junctions (4WJ) have never been analysed. RNA 4WJs belong to the different junctions which are common architectural features in RNA; they play a role in RNA folding which is a critical feature in the regulation of any RNA activity. RNA 4WJs show a higher diversity with respect to those based on DNA, with a continuous interconversion between parallel and antiparallel conformations,[21] whereas DNA 4WJs typically adopt a fixed antiparallel structure. Recent studies by some of the authors of the present work have shown that the $[Pt(H_2bapbpy)]^{2+}$ complex (where $H_2bapbpy$ = H_2L1 is N-(6-(6-(pyridin-2-ylamino)-pyridin-2-yl)pyridin-2-yl)pyridin-2-amine) can drive the crystallization of a DNA oligomer into a 4WJ-like motif.[22] Therefore, it seemed interesting to study the possible binding of Pd(II) analogues of this Pt(II) complex to RNAs polynucleotides and an RNA 4WJ. Natural DNA and DNA G-quadruplexes were also considered for comparison. The structures of the metal complexes considered in this work are shown in Figure 1: starting from the already cited $[Pt(H_2L1)]Cl_2$ complex, the logic is to analyse how the change in the geometry/rigidity of the tetradentate ligand or a different metal centre may modulate the reactivity with different nucleotide substrates.

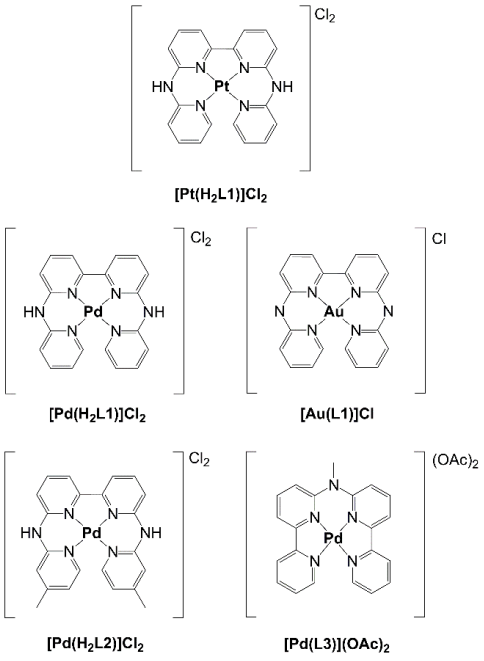

Figure 1 – Molecular structures of the analysed complexes.

2 Materials and Methods

2.1 Materials

2.1.1. Metal complexes. The metal complexes were synthesised, purified and characterised according to an already published procedure (for Au(L1)Cl manuscript in preparation).[22, 23] The molar concentration of the metal complex (i.e. dye, drug) will be indicated as C_D. The stock solutions of the complexes were obtained by dissolving weighted amounts of the solid in DMSO to ca. 3 mM. Given that the counter-ion is released in solution, the species will be expressed from now on as the charged reacting species all along the text, with the exception of the ESI mass spectrometry tests. Working solutions were obtained by diluting the stock in the buffer (all along the text NaCl 0.1 M, NaCac 2.5 mM, pH 7.0 if not otherwise cited, Cac = cacodylate) to such an extent that the DMSO content is negligible. Ethidium bromide (Merck, purity > 99%, ε(480 nm) = 5800 M^{-1} cm^{-1}, intercalator),[24, 25] thiazole orange methyl sulphate (TO, Merck, purity 90%, intercalator),[26, 27] 5,10,15,20-Tetrakis(1-methyl-4-pyridinio) porphyrin tetra(p-toluenesulfonate) (Merck, purity 97%, G4 stabiliser),[28] coralyne chloride (Merck, purity 99%, groove binder/half intercalator)[29] are reference dyes whose binding mode to nucleic acids is known and whose solutions (stock ca. 1 mM) where prepared by weight in buffer and kept in the dark at 4 °C.

2.1.2 Polynucleotides. As for RNAs, poly(rA) and poly(rU) were from Sigma-Aldrich; both polyribonucleotides were weighted, dissolved in the buffer and their molar concentration was checked using ε(257 nm) = 10110 cm^{-1} M^{-1} for poly(rA) and 8900 $cm^{-1}M^{-1}$ for poly(rU).[30] Double-stranded poly(rA)·poly(rU) (ca. 1 mM in base pairs) was obtained from 1:1 mixing of the single strands and overnight equilibration in the dark at room temperature. Similarly, for triple-stranded poly(rA)·2poly(rU) formation, an equimolar amount of poly(rU) is added to poly(rA)·poly(rU), the mixture is left to equilibrate overnight in the dark at room temperature (molar concentration in base triplets). Literature data confirm that this procedure is sufficient to ensure helices formation.[31] The final molar concentration of poly(rA)·poly(rU) is given in base pairs, that of poly(rA)·2poly(rU) in base triplets. As for the DNAs studied for comparison purposes, double-stranded calf thymus DNA (CT-DNA, B-form) was from Sigma (highly polymerised, sodium salt). Prior to use, DNA solid is dissolved in the buffer and sonicated as to reduce the polynucleotide length to ca. 500 base pairs, according to an already described procedure.[32] The molar concentration of the polynucleotide solutions, expressed as base pairs, is calculated spectrophotometrically as $C_P = A_{260}/13200$ where A_{260} is the absorbance at 260 nm in a 1.0 cm cuvette and 13200 M^{-1} cm^{-1} the relevant molar extinction coefficient for base pairs.[33]

2.1.3 Oligonucleotides. The RNA four-way junction (RNA-4WJ) is obtained by the folding of four filaments expressly designed to ensure the correct final geometry (Figure 2). The seller (Metabion International AG) provided the single filaments as dry salts with HPLC purification (Condalab); they are named as b, r, h and x filaments whose sequence is: b: 5'-CCU AGC AAG

CCG CUG CUA CC-3'; r: 5'-CCA CCG CUC UUC UCA ACU GC-3'; h: 5'-GGU AGC AGC GAG AGC GGU GG-3'; x: 5'-GCA GUU GAG AGC UUG CUA GG-3'. The choice of the sequence has been done following the paper by Duckett et al..[34]

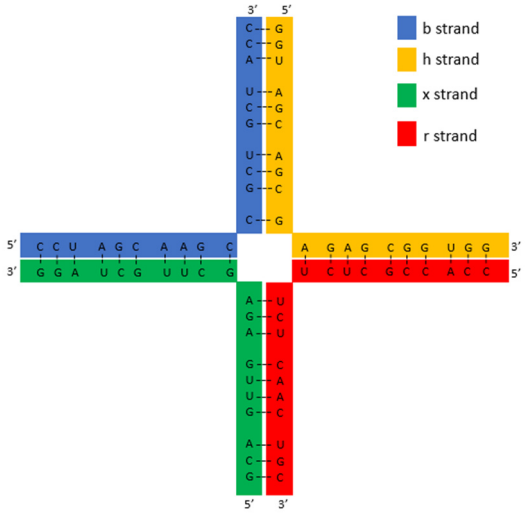

Figure 2 – Schematic drawing of the RNA four-way junction used in this work with relevant base sequences/pairings.

The preparation of the stock solution of RNA-4WJ is done first by adding 10 × nmol microliters (µL) of ultra-pure water in each of the strand vials, where nmol is the nanomole content in strands in the vial, known from the sample certificate. The exact amount of µL needed is obtained by a micro-syringe connected to a Mitutoyo micrometric screw (1 turn of the screw = 8.2 µL). This produces 100 µM solutions of each of the strands. By mixing the same volume of each of the four strands, we obtain a 25 µM solution of RNA-4WJ which is annealed following a protocol which establishes (a) slow heating in a water bath until 90 °C, (b) 10 min at 90 °C, (c) slow cooling until room temperature. The detailed analysis of the influence of the role of metal ions in the conformation of RNA-4WJ (done on the same sequence used here) suggests that second group salts (in particular $MgCl_2$ or $CaCl_2$) are needed to stabilise the 4WJ and may be tuned to obtain the desired geometry.[34] Preliminary melting tests in the ranges suggested by this study, let us choose 180 µM $CaCl_2$ as the medium for the here presented RNA-4WJ experiments for better data reliability and reproducibility. The stability of a mixture of the four strands (T_m = 43 °C) is significantly higher than what occurs when only two over four strands are mixed (T_m = 33 °C): this confirms the formation of the 4WJ (Figure S1). NUPACK (https://nupack.org/) software returned quantitative formation of the 4WJ only, also at concentrations as low as 0.025uM, with energy of ca. -300 kJ/mol in water.[35] On the whole, these data indicate that the 4WJ is a very stable form, at least largely majority under our experimental conditions.

The DNA G4 selected for testing is called CTA-22 (5'-AGG GCT AGG GCT AGG GCT AGG G-3') and is a chair-type antiparallel DNA human telomere (Protein Data Bank entry 2KM3) which contains two G-tetrad layers and a G-C-G-C tetrad and that was shown to have interesting biophysical properties.[36-38] It was dissolved in a KCl 0.1 M, LiCac 2.5 mM, pH = 7.0 buffer (molar concentration ca. 2 mM in strands) and then annealed according to the same procedure cited above for RNA-4WJs.

2.1.4 Buffers. The aqueous buffer used was NaCl 0.1 M, NaCac 2.5 mM (Cac = cacodylate) pH = 7.0, with the exception of the melting experiment with CT-DNA where the buffer was NaCac 2.5 mM pH = 7.0. For the experiments with G4s the buffer was KCl 0.1M LiCac 2.5mM pH 7.0 for the titrations and melting analysis, while for the mass spectrometry the buffer was NH_4OAc 0.1M pH 7.0. Ultra-pure water from an ultra-pure Sartorius Arium-pro purification system was used throughout. Common reagents were the commercial analytical grade compounds and were used as received.

2.2 Methods

2.2.1 Spectrophotometric measurements. The experiments were performed on a double beam Shimadzu 2450 apparatus, equipped with jacketed cell holders for temperature control to within ± 0.1 °C. The instrument enables temperature programs for melting experiments (used one is 5 °C change at 5 °C/min rate + 5 minutes hold time). Cuvettes of 1.0 cm, 2.0 mm or 1.0 mm light path were used depending on the experiments. A short light path was needed in particular for the oligo (RNA 4WJ and DNA G4) melting tests. UV-vis titrations are made by adding known amounts of the biosubstrate to the metal complex (ca. 2×10^{-5} M) directly into the spectrophotometric cell. The additions are done using a gas-tight Hamilton syringe connected to a Hamilton micrometric screw (one turn is 8.2 µM, the minimum addition possible is 1/50 of a turn). Spectrofluorometric measurements were done on a Perkin Elmer LS55 apparatus, equipped with jacketed cell holders for temperature control to within ± 0.1 °C. Fluorescence titrations were done according to the same addition procedure explained above for UV-vis, the metal complexes concentrations are here 10 µM. In the EtBr exchange tests, DNA is first saturated with this fluorescent intercalator by adding increasing amounts of the dye to the polynucleotide, directly in the spectrofluorometric cell. This pre-titration is stopped as soon as the fluorescence increase starts to level out (λ_{ex} = 520 nm, λ_{em} = 595 nm), to ensure saturation but to avoid free dye excess. Second, the metal complex is added to the mixture. EtBr is practically non-fluorescent in the buffer but strongly fluorescent when DNA-bound. Fluorescence decrease indicates EtBr environment changes.

2.2.2 Viscometric tests. Viscometry measurements are done using a semi-micro "Cannon-Ubbelohde" capillary viscometer, placed in a water bath at a constant temperature (25.0 ± 0.1 °C). In these experiments, 3.0 mL of CT-DNA are mixed with increasing amounts of either the buffer alone or metal complex in buffer solution. The flow time within the capillary is measured by a stopwatch. The relative viscosity is calculated using according to $\eta/\eta^\circ = (t_{sample}-t_{solv})/(t_{DNA}-t_{solv})$, where t_{sample} is the flow time of the metal complex/DNA mixture, t_{DNA} is the

time of DNA at the same concentration as the sample, and t_{solv} is the time of the buffer. The polynucleotide elongation will be proportional to the third root of η/η°. The capillary is carefully washed following a cycle requiring water, acetone, water, ethanol and, finally, nitrogen flow.

2.2.3 ESI mass spectrometry. For the mass spectrometry measurements, all samples were prepared in LC-MS grade solvents or solutions. The G4 containing solution (10^{-3} M) was prepared according to the procedure already described,[39] in 0.1 M ammonium chloride solution (pH 7.0). For the reaction with the selected metal complex, an aliquot of the G4 stock solution was mixed with an aliquot of the $3x10^{-3}$ M metal complex stock solution in DMSO and diluted with 0.1 M ammonium acetate solution (pH 7.0) to a final G4 concentration of 10^{-5} M. The G4 to metal complex molar ratio was 1:3. The obtained mix was incubated for 24 h at 37 °C. Just before the direct infusion into the mass spectrometer, the mixture was further diluted with 40:60 water/ethanol solution to a final G4 concentration of 10^{-6} M. The high-resolution ESI mass spectra were recorded using an AB SCIEX Triple TOF 5600+ (Sciex, Framingham, MA, USA), equipped with a DuoSpray® interface operating with an ESI probe. All the ESI mass spectra were acquired through a direct infusion at 5 µL min^{-1} flow rate. The ESI source parameters were optimized as follows: negative polarity, ion spray voltage floating -4500 V, temperature 25 °C, ion source gas 1 (GS1) 35 L min^{-1}; ion source gas 2 (GS2) 0 L min^{-1}; curtain gas (CUR) 20 L min^{-1}, declustering potential (DP) -250 V, collision energy (CE) -10 V, acquisition range 1100-2800 m/z. For acquisition, Analyst TF software 1.7.1 (Sciex) is used and deconvoluted spectra were obtained by using the Bio Tool Kit micro-application v.2.2 embedded in PeakView™ software v.2.2 (Sciex).

3 Results

3.1 Spectroscopic characterisation and aggregation tendency evaluation

To characterise the metal complexes under study, UV-vis spectra at different concentrations in buffer (10^{-7} M – 10^{-4} M range) were first recorded. The linearity of the absorbance *vs.* compound concentration was verified, and spectra at different temperatures were taken. The absence of aggregation processes should result in the absence of spectrum profile changes at increasing concentrations or temperatures, the linearity of absorbance *vs.* concentration plots and the constancy of the ratio of absorbance values at different wavelengths. These tests are important as dye-dye interactions may affect the subsequent discussion on binding to polynucleotides. These data are provided in the Supporting Information as Figures S2 – S6. Overall, it was found that $[Pd(H_2L1)]^{2+}$, $[Pd(H_2L2)]^{2+}$ and $[Pt(H_2L1)]^{2+}$ undergo some self-aggregation under these conditions, but that $[Pd(L3)]^{2+}$ and $[Au(L1)]^{+}$ do not. These data confirm that the metal centre and the ligand geometry/steric hindrance heavily modulate the dye-dye interaction. Note that the $[Pd(H_2L1)]^{2+}$, $[Pd(H_2L2)]^{2+}$ and $[Pt(H_2L1)]^{2+}$ complexes undergo acid-base equilibria with release of H^+ from the ligand. However, the pK_A values involved are ≥ 7.8. Accordingly, the spectra of the complexes under the experimental conditions used in this work agree with the fully protonated species only (manuscript in preparation).

3.2 RNA polynucleotides binding

Spectrophotometric titrations were carried out where increasing amounts of the RNA duplex or triplex were added to the metal complex solution. The very significant changes observed in the absorbance profile (Figure 3 and Figure S7) indicate that some form of interaction does indeed take place for all systems. According to a simplified model, where a nucleotide reacting unit (base pair/triplet/G4) interacts with one complex molecule (dye, drug) according to Equation (1)

$$P + D \leftrightarrows PD \quad (1)$$

the relevant binding constant, K_{app}, can generally be evaluated according to Equation (2)

$$\frac{\Delta A}{C_D} = \frac{\Delta\varepsilon K_{app}[P]}{K_{app}[P]+1} + a \quad (2)$$

where $\Delta A = A - \varepsilon_D C_D$, $\Delta\varepsilon = \varepsilon_{PD} - \varepsilon_D$, ε_i is the molar extinction coefficient of the i-species, [P] is the free (non-complexed) base pair/triplet/G4, and a is an offset. K_{app} is an apparent equilibrium constant as it has to account also for possible metal complex self-aggregation.[36] Note that the calculation requires an iterative procedure as [P] is not known. Thus, first $[P] = C_P$ is set, in order to obtain a first K_{app} approximation. Then, this K_{app} value is used to evaluate [PD] and $[P] = C_P - [PD]$, the latter being used to re-plot the data and obtain a better K_{app} estimate. The procedure is repeated until convergence. Table 1 reports the data collected; they immediately point out that the binding affinity is the intricate result of the interaction between the ligand, the metal centre, and the substrate.

On those systems which do not undergo auto-aggregation ($[Pd(L3)]^{2+}$ and $[Au(L1)]^{+}$) the binding constant can be evaluated also according to a McGhee and von Hippel fitting.[40] This enables to evaluate not only the binding constant in the absence of dye-dye aggregation in solution (K) but also n, the number of base pairs/triplets involved in the binding of one molecule ("site size"). The results of this fitting are shown in Table 2. A value of n slightly higher than 1 corresponds to the "excluded site" model for total intercalation by Lerman;[26, 41] on the other hand, the n values significantly lower than 1 in the case of the $[Pd(L3)]^{2+}$/poly(rA)poly(rU) and $[Pd(L3)]^{2+}$/poly(rA)2poly(rU) systems ($n \cong 0.5$ would mean two dye molecules for each of the base pairs/triplets) hint for some partial intercalation mode where the part which remains out of the helix undergoes some dye-dye interaction.

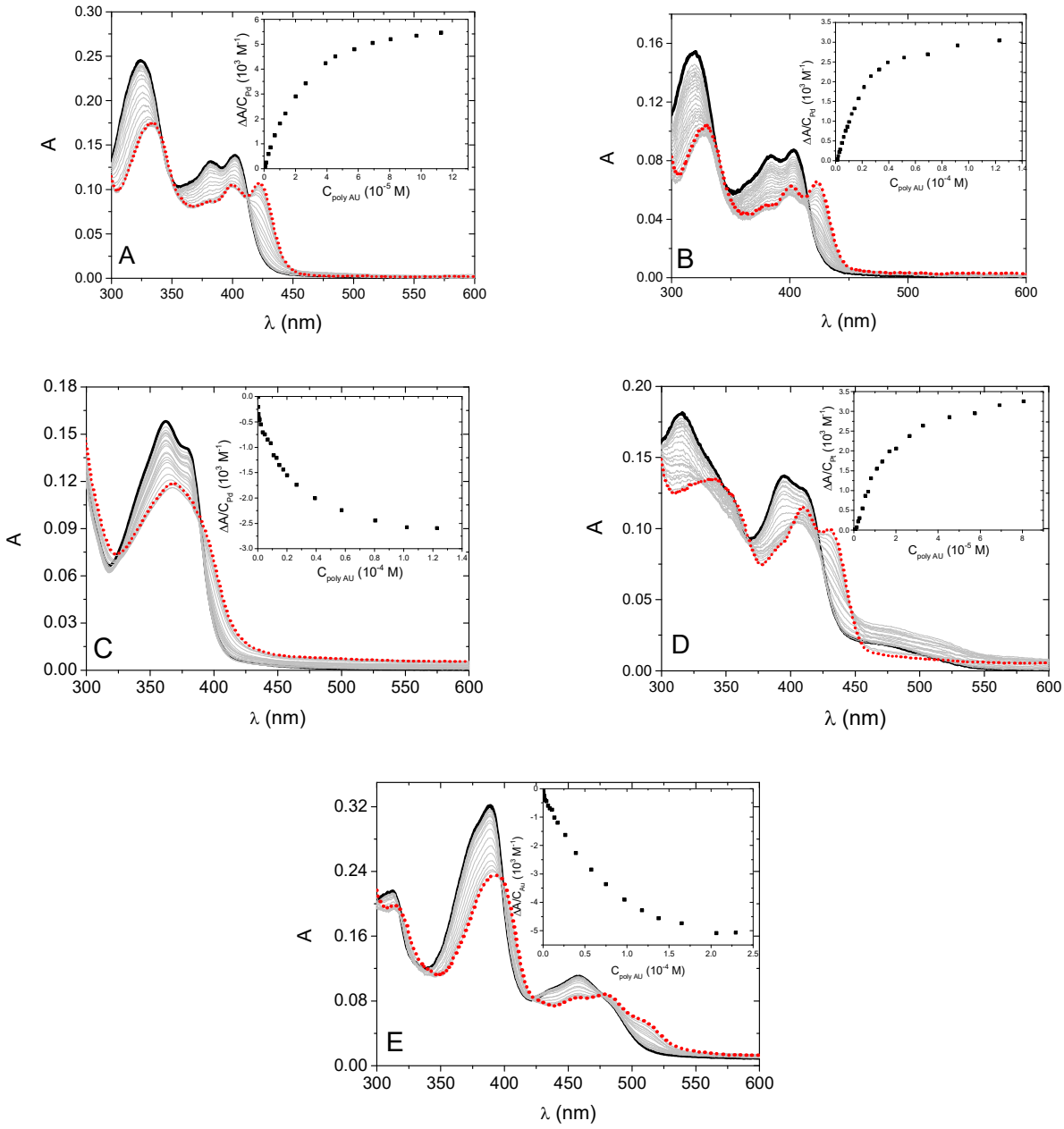

Figure 3 – UV-vis titrations with poly(rA)·poly(rU), NaCl 0.1 M, NaCac 2.5 mM, pH 7.0, 25.0 °C. (A) $[Pd(H_2L1)]^{2+}$/poly(rAU) system, C_{Pd} = 1.44×10^{-5} M, C_{polyAU} from 0 M (—) to 1.13×10^{-4} M (.....), the inset is the binding isotherm at λ = 425 nm; (B) $[Pd(H_2L2)]^{2+}$/poly(rAU) system, C_{Pd} = 1.37×10^{-5} M, C_{polyAU} from 0 M (—) to 1.23×10^{-4} M (.....), the inset is the binding isotherm at λ = 423 nm; (C) $[Pd(L3)]^{2+}$/poly(rAU) system, C_{Pd} = 1.68×10^{-5} M, C_{polyAU} from 0 M (—) to 1.23×10^{-4} M (.....), the inset is the binding isotherm at λ = 363 nm; (D) $[Pt(H_2L1)]^{2+}$/polyAU system, C_{Pt} = 1.72×10^{-5} M, C_{polyAU} from 0 M (—) to 8.06×10^{-5} M (.....), the inset is the binding isotherm at λ = 434 nm; (E) $[Au(L1)]^{+}$/poly(rAU) system, C_{Au} = 1.74×10^{-5} M, C_{polyAU} from 0 M (—) to 2.29×10^{-4} M (.....), the inset is the binding isotherm at λ = 388 nm.

Table 1. Binding constants for different metal/nucleic acid systems at 25.0 °C calculated with equation (2). NaCl 0.1 M, NaCac 2.5 mM, pH = 7.0; for G-quadruplex the buffer is KCl 0.1 M, LiCac 2.5 mM, pH 7.0; +∞ = quantitative aggregation on the nucleotide/cooperative reaction.

	K_{app} (10^4 M^{-1})				
	$[Pd(H_2L1)]^{2+}$	**$[Pd(H_2L2)]^{2+}$**	**$[Pd(L3)]^{2+}$**	**$[Pt(H_2L1)]^{2+}$**	**$[Au(L1)]^{+}$**
Auto-aggregation	*yes*	*yes*	*no*	*yes*	*no*
poli(rA)·poli(rU)	6.7±0.2	9.3±0.3	16±2	27±2	1.4±0.1
poli(rA)·2poli(rU)	2.5±0.5	12±1	50±5	17±3	5.4±0.5
CT-DNA	1.0±0.1	1.1±0.1	3.4±0.5	+∞	0.58±0.07
G-quadruplex	+∞	+∞	+∞	+∞	30±2

Table 2. Binding constants for different metal/polynucleotide systems at 25.0 °C calculated according to a McGhee and von Hippel fitting.[40] NaCl 0.1 M, NaCac 2.5 mM, pH = 7.0.

	$[Pd(L3)]^{2+}$		$[Au(L1)]^{+}$	
	K (10^4 M^{-1})	n	K (10^4 M^{-1})	n
poli(rA)·poli(rU)	8.1±0.3	0.6±0.3	1.7±0.1	1.4±0.1
poli(rA)·2poli(rU)	20±2	0.5±0.2	7.6±0.9	1.2±0.1
CT-DNA	5.7±0.5	1.3±0.2	0.51±0.05	1.2±0.6

The affinity for the RNA polynucleotides was further investigated using melting tests (Figures 4 and S8, Table S1). A change of more than 30 °C in the melting temperature (°C) of the drug/RNA mixture, compared to RNA only (ΔT_m), can be interpreted as a very large stabilisation. The stabilisation of poly(rA)2poly(rU), even if lower than the double stranded counterparts, remained high. This fact, together with the high K_{app} values for poly(rA)2poly(rU), indicates that the third strand does not significantly prevent binding. As in the triplex the wide groove is hindered by the third strand, this observation would suggest that the binding occurs principally in the minor groove. The experiments based on the displacement of the EtBr fluorescent intercalator (see 2.2.1) confirmed interaction between the metal complexes and the polynucleotide and demonstrated that the qualitative trend of the insertion strength was $[Pd(H_2L1)]^{2+} \cong [Pd(H_2L2)]^{2+} > [Pt(H_2L1)]^{2+} \cong [Au(L1)]^{+} > [Pd(L3)]^{2+}$ (Figure S9).

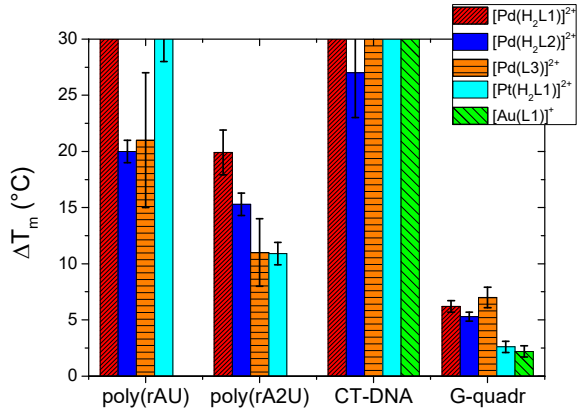

Figure 4 – Difference of the melting temperature between the metal complex/nucleotide mixture and the nucleotide alone, $\Delta Tm = T_m$(complex/nucleotide) – T_m(nucleotide). NaCl 0.1 M, NaCac 2.5 mM, pH = 7.0 for poly(rA)poly(rU) and poly(rA)2poly(rU); NaCac 2.5 mM, pH = 7.0 for CT-DNA; KCl 0.1 M, LiCac 2.5 mM, pH = 7.0 for G4. For both $[Au(L1)]^{+}$/poly(rA)poly(rU) and $[Au(L1)]^{+}$/poly(rA)2poly(rU) systems $\Delta Tm \cong 0$.

3.3 CT-DNA binding

For comparison with RNAs, absorbance titrations and melting test were repeated using natural calf thymus DNA (CT-DNA) as substrate; EtBr exchange tests and viscometric titrations were performed as well. Overall, absorbance titrations confirmed the binding of the complexes to DNA (Figure S10). Interestingly, Table 1 shows that the affinity of all the complexes is lower for double-stranded DNA with respect to both double and triple-stranded RNAs. Viscometric data (Figure S11) show that [Au(L1)]Cl is the species that is able to more deeply insert between base pairs and produces the higher double helix elongation. On the whole, the insertion degree will be $[Au(L1)]^{+} > [Pd(L3)]^{2+} > [Pd(H_2L1)]^{2+} \cong [Pt(H_2L1)]^{2+}$. For $[Pd(H_2L)]^{2+}$ it may be speculated that the methyl groups drive a geometrical distortion and, thus, a partial intercalation mode which would turn into some helix compaction (viscosity decrease). The very similar changes in the metal complex spectral profile upon metal complex/nucleotide interaction suggest that the binding mode is mainly the same (total/partial intercalation) for DNA and RNAs with an efficacy tuned by geometrical changes.

An exception is $[Pt(H_2L1)]^{2+}$, the polynucleotide-bound absorbance profile of which is greatly different between DNA and RNAs (compare Figures 3D – S7D – S9D). This observation agrees with the existence of a quantitative/cooperative binding for the $[Pt(H_2L1)]^{2+}$/CT-DNA binding (Table 1). Such features may be related to aggregation of the platinum complex on the polynucleotide template, which would occur on the DNA grooves and not in the RNAs ones. To confirm this point, CD spectra of the $[Pt(H_2L1)]^{2+}$/CT-DNA system (and $[Pd(H_2L1)]^{2+}$/CT-DNA for comparison) were collected (Figure S12). In the case of $[Pt(H_2L1)]^{2+}$, a bisignate induced circular dichroism (ICD) signal in the > 300 nm range and the sign conversion of the DNA band at 275 nm concur in indicating strong dye-dye interactions and formation of supramolecular DNA aggregates.[42, 43] On the contrary, $[Pd(H_2L1)]^{2+}$/CT-DNA shows a very different shape, with a significant but limited 275 nm band change and a negative ICD band, both features being in line with intercalation.[42]

3.4 G-quadruplex binding

The affinity of this family of complexes for G4 structures (CTA-22 sequence, antiparallel DNA human telomere) was also evaluated by means of absorbance titrations (Figure S13) and melting tests (Figure 5).

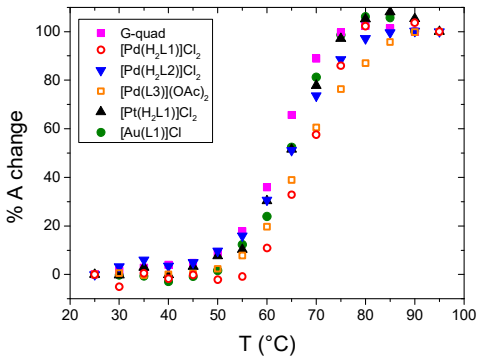

Figure 5 – Melting tests for CTA-22 alone (squares), $[Pd(H_2L1)]^{2+}$/CTA-22 (open circles), $[Pd(H_2L2)]^{2+}$/CTA-22 (down triangles), $[Pd(L3)]^{2+}$/CTA-22 (open squares), $[Pt(H_2L1)]^{2+}$/CTA-22 (up triangles), $[Au(L1)]^{+}$/CTA-22 (circles); $C_{CTA22} = C_D = 1.20\times10^{-5}$ M, r_b = complex/CTA-22 = C_D/C_P = 1.0, % A change = 100*(A – A°)/(A∞ – A°) where A° and A∞ are the two absorbance values limiting the fitting sigmoid; KCl 0.1M, LiCac 2.5 mM, pH 7.0, λ = 295 nm.

The significant changes in the absorbance profiles upon mixing indicated that an interaction is taking place. However, with the exception of the $[Au(L1)]^+$/G4 system, the reaction turned out to be quantitative (Table 1). Again, excluding the case of the $[Au(L1)]^+$/CTA-22 system, the titration was already finished at a ratio between reactants $C_{CTA22}/C_{complex}$ << 1, indicating aggregation of the metal complex on the oligo G4 structure. Melting tests showed some non-negligible stabilisation of the oligonucleotide upon adduct formation (see also Figure 5). This strong interaction was hence further inspected by means of ESI mass spectrometry**.** Indeed, during the last two decades, mass spectrometry has emerged as one of the most powerful tools to analyse both covalent and non-covalent interactions between metal-based complexes and biomolecules.[44-47] In particular, thanks to the very soft ionization conditions that permit not only to prevent sample fragmentation, but also to retain the native conformations of the biomolecules, the ESI technique has become the election technique for the analysis of proteins,[48, 49] DNA/RNA fragments[50, 51] and their non-canonical structures like the G4 one.[39, 52-54]

In the present work, we applied the ESI MS technique to confirm the presence of intercalative interactions between the metal complexes and the G4 structure. Hence, the CTA-22 single-stranded DNA was firstly annealed, following the already described procedure,[39] leading to the respective parallel-stranded G4 DNA. The annealing process has been carried out in an ESI-friendly aqueous solvent containing the monovalent cation NH_4^+ in the place of K^+. In fact, the ionic radii of these two ions are very similar (1.48 and 1.33 Å, respectively) and lead to the same placement of these cations between the tetrads' planes.[55, 56] The ESI mass spectrum was then recorded in order to verify the proper formation of the G4 structure. The spectrum (see Figure S14) shows a signals cluster at 6937.358, 6954.347, 6975.375 and 6998.323 Da that was in perfect agreement with the CTA-22 molecular mass plus up to four ammonium ions, which promote the G4 assembly and are accommodated inside the structure.[52, 56-59] The presence of these ammonium ions is straightforward information that the G4 structure was present and retained during the electrospray ionisation process. Beyond this cluster, a much less intense peak was still visible at 6920.322 Da, corresponding to a residual amount of the CTA-22 single-stranded DNA.

Subsequently, the obtained G4 was incubated for 24h with each of the metal complexes and the mass spectra of the respective solutions were recorded. Figure 6 shows the spectrum obtained for $[Pd(L3)](OAc)_2$. In this spectrum, two major clusters of peaks were observed, one at 7382.405 Da and the second at 7824.483 Da. Also in this case, both clusters showed the characteristic distribution of ammonium ions, which have been omitted in the figure for a better readability but confirm the retention of the G4 structure. Both clusters were mass-shifted according to the nature and stoichiometry of the formed metal adduct, highlighting the retention of the G4 folding during the reaction.

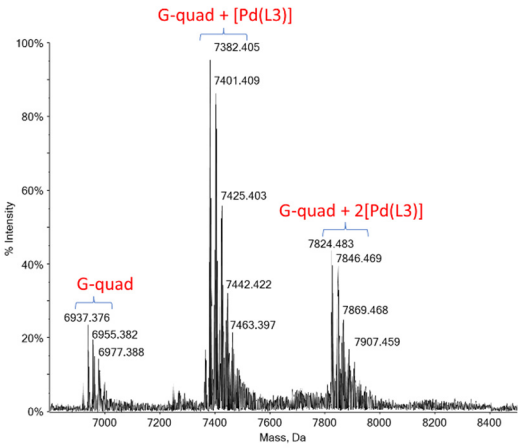

Figure 6 – Deconvoluted ESI mass spectrum of 10^{-6} M G4 incubated for 24 h with $[Pd(L3)](OAc)_2$ in 100 mM ammonium acetate solution (pH 7.0) and in the presence of 60% EtOH. 3:1 metal complex/G4 molar ratio. The distribution of the ammonium ions has been omitted for clarity.

Moreover, a simple reactivity pattern emerged highlighting the binding (probably via intercalation) of, respectively, one and two cationic metal complexes between the G4 tetrads. In this spectrum, a small cluster was also present, with the most abundant signal at 6937.376 Da, corresponding to a residual amount of unreacted, but still folded, G4. A very similar reactivity pattern was obtained for $[Pd(H_2L1)]Cl_2$ (see Figure S15), which showed a little more intense intercalative behaviour with respect to the previous compound, giving rise to a more pronounced reactivity and to the formation of adducts characterised by the presence of maximum three metallic fragments per G4 molecule. On the other hand, the spectrum recorded for the Pt-containing analogue, i.e. $[Pt(H_2L1)]Cl_2$, and reported in Figure S16, shows the formation of only one adduct with the G4, with a 1:1 stoichiometric ratio. Although even in this case the interaction with the biomolecule involves the cationic metallic fragment with the complete retention of the organic ligands, probably the presence of a different metal centre causes an appreciable lowering in the overall reactivity. Moreover, in the case of the platinum complex, a significant amount of unreacted G4 and some unfolded CTA-22 were also present.

The reactivity of [Au(L1)]Cl was much more complicated (Figure 7). Probably, the presence of the Au(III) centre could trigger some redox equilibria during the reaction with the biomolecules leading to the consequent release of Au(I) ions. This reactivity behaviour is characteristic and quite common for Au(III)-based compounds and it has been well described in the literature.[60-62] Here, the spectrum shows three low-intensity peak clusters (labelled at 7133.375, 7669.453 and 8201.568 Da), all of them pointing out the presence of G4 adducts with Au ions deprived of the organic ligands. Furthermore, like for the Pd and Pt compounds the high-intensity peaks could be assigned to the mono and bis-adduct of the G4 with the $[Au(L1)]^+$ cationic fragment. These peaks showed a significantly lower intensity than that of the free G4, suggesting an overall lower interaction degree of the gold compound, compared to its Pd and Pt analogues.

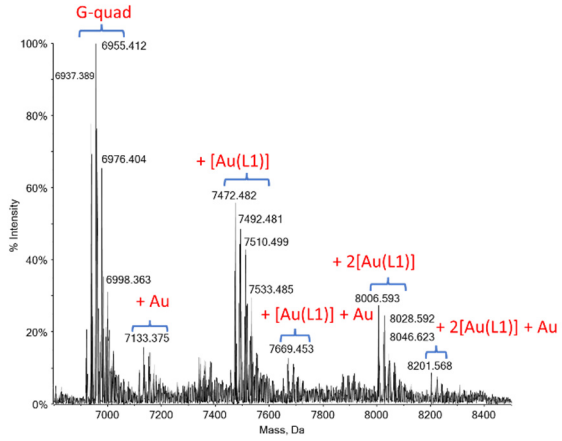

Figure 7 – Deconvoluted ESI mass spectrum of 10^{-6} M G4 incubated for 24 h with [Au(L1)]Cl in 100 mM ammonium acetate solution (pH 7.0) and in the presence of 60% EtOH. 3:1 metal complex/G4 molar ratio.

Interestingly, as depicted in Figure S17, ligand loss was also observed for $[Pd(H_2L2)]Cl_2$. In contrast with the results obtained for [Au(L1)]Cl, however, in this spectrum the signals belonging to the adducts with one or two molecules of $[Pd(H_2L2)]^{2+}$ were sensibly less intense compared with those containing the naked Pd ion. Unfortunately, at this stage of the research is not possible to define the metal oxidation state for the bare Au and Pd ions involved in the adduct formation with the G4. However, the much greater lability of Pd(II) complexes compared to Pt(II) analogues is well documented and supports the possibility of a rapid ligand release in solution.[63] Noteworthy, $[Pd(H_2L2)]Cl_2$ differs from the other Pd-containing analogue $[Pd(H_2L1)]Cl_2$ only by the presence of the two methyl groups on the pyridyl moieties of the ligand. Probably, this structural difference is responsible for the different reactivity patterns of the two compounds and for the greater propensity of $[Pd(H_2L2)]Cl_2$ to lose the organic ligand.

In conclusion, mass spectrometry experiments highlight that both adducts of the metal ion alone, or of 1, 2, or 3 metal complexes, can be observed interacting with the G4. Overall, both the nature of the metal centre and the ligand geometry influence the reactivity of this type of metal complexes.

3.5 RNA 4WJ interactions

Coming back to the main focus of our work, we switched from the RNA polynucleotides above to the analysis of the possible binding to peculiar RNA oligos. In this frame, as already cited in the introduction paragraph, RNA four-way junctions deserve much interest as a possible specific anticancer drug target. They have an active role in RNA folding but, to the best of our knowledge, no information about metal complexes binding are available. Absorbance titrations for the different metal complex/RNA-4WJ systems are shown in Figures S18 ($[Pd(H_2L1)]^{2+}$, $[Pd(L3)]^{2+}$ and $[Pt(H_2L1)]^{2+}$) and Figure 8 ($[Au(L1)]^{+}$). Given the tendency of $[Pd(H_2L2)]^{2+}$ for losing its ligand in solution, this complex was discarded from our studies with the delicate RNA-4WJ substrate. The spectral profile changes indicate the presence of an interaction in all four cases. This is not surprising as the RNA-4WJ junction contains four double-stranded RNA appendices. Thus, some dye binding may occur here, as already evidenced by the experiments with poly(rA)poly(rU). On the other hand, a different behaviour with respect to what was already observed for the polynucleotide would suggest specific binding to the RNA-4WJ. Such an observation was made for the $Au(L1)]^{+}$ complex, where the spectral evolution upon RNA-4WJ addition differed from what was observed for poly(rA)poly(rU) titrations (compare Figure 3E with Figure 8A). Also, binding to RNA-4WJ did not generate the same spectroscopic signature as when two only (x and r) coupled strands were added (Figure 8A-C).

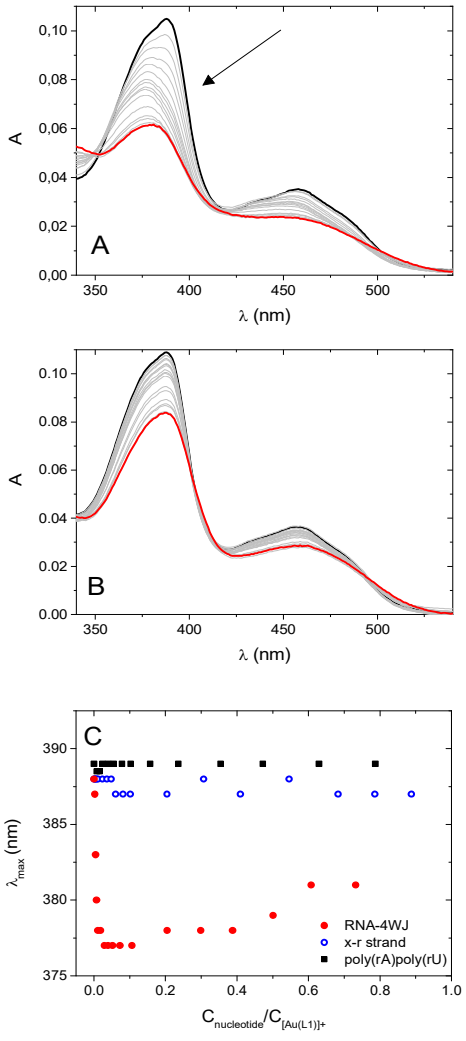

Figure 8 – UV-vis titrations $[Au(L1)]^{+}$ (C_{Au} = 6.36×10^{-6} M) with RNA oligonucleotides, $CaCl_2$ 182 μM, pH 7.0, T = 25.0 °C. (A) $[Au(L1)]^{+}$/RNA-4WJ system, C_{RNA4WJ} from 0 M (—) to 4.65×10^{-6} M (.....); the arrow points to the $[Au(L1)]^{+}$ band which, interestingly, upon RNA-4WJ increase, undergoes first a blue and then a red shift.; (B) $[Au(L1)]^{+}$/xr strand system, $C_{xrstrand}$ from 0 M (—) to 4.54×10^{-6} M (.....); (C) position of the absorption maximum (nm) of $[Au(L1)]^{+}$ as a function of the nucleotide added for addition of RNA-4WJ (full red circles), x-r stand (open blue circles) or poly(rA)·poly(rU) (black full squares).

Beyond an hypochromic effect observed for all poly(rA)poly(rU), x-r two-strands and RNA-4WJ, only in the case of RNA-4WJ the band peaked at around 380 nm (and also at around 450 nm but it is here less visible) undergoes a shift of the position of the maximum and, thus, changes the form of the absorbance profile (Figure 8A). There are two opposite shifts (first blue, then redshift) which suggest the formation of two types of adducts: Figure 8C emphasises this behaviour by plotting the position of the maximum against the nucleotide content. The same panel shows that these shifts happen only for the RNA-4WJ and not for RNA polynucleotides nor x-r two-strands coupling.

Melting tests were done on RNA-4WJ systems. The mixtures were heated, cooled down slowly until r.t. and then re-heated a second time. This procedure enables to enlighten possible peculiar adduct geometries which become accessible only when the junction is opened. The same experiments were repeated also using known reference dyes as ethidium bromide (EtBr, known double strands intercalator producing significant helix unwinding)[24], thiazole orange (TO, intercalator),[64] coralyne (Co, groove/partial intercalator with ability to induce RNA triplexes[65] and 5,10,15,20-tetrakis(1-methyl-4-pyridyl)-21H,23H-porphine (TMPyP4, groove binder, which also strongly binds to G4 tetrads.[28] Figure 9 shows the results: it can be observed that there are two different behaviours. (A) EtBr, TO and Co undergo reversible binding modes and produce a RNA-4WJ stabilisation which is reproducible over the two consecutive runs; (B) TMPyP4 first stabilises the system, then places itself in a position which strongly destabilises the RNA-4WJ in the second run. $[Pt(H_2L1)]^{2+}$ and $[Pd(L3)]^{2+}$ belong to type (A), whereas $[Pd(H_2L1)]^{2+}$ and $[Au(L1)]^{+}$ belong to type (B). However, $[Au(L1)]^{+}$ stabilises also the x-r double stranded coupling, whereas any stabilisation effect was lost in the $[Pd(H_2L1)]^{2+}$/x-r system (Figure S19). Overall, both $[Pd(H_2L1)]^{2+}$ and $[Au(L1)]^{+}$ seem to show peculiar interactions related to the RNA-4WJ junction. These species will be the subject of further investigations in the future.

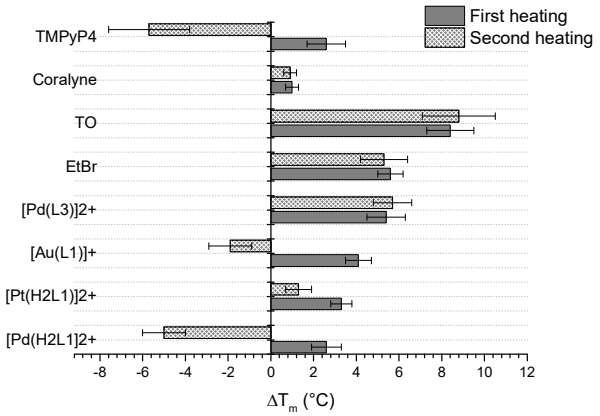

Figure 9 – Melting temperature difference (ΔTm, °C) between that of a drug/RNA-4WJ mixture and that of the RNA-4WJ alone; C_{drug} = 20 μM, C_{RNA4WJ} = 10 μM, $CaCl_2$ 182 μM, pH 7.0.

Conclusions

According to this study, all tetrapyridyl d^8 metal complexes do interact with RNA (and DNA) fragments, but the exact features of this interaction are in each case the result of a complex structure-reactivity relationship (SAR) involving both the ligand, the metal centre, and the polynucleotide. The different metal centre and/or the ligand produces planar geometries with different distortion degrees. An higher planarity may produce two opposite effects: on the one hand, it favours intercalation between DNA base pairs, and on the other hand, it favours (also on the polynucleotide grooves) dye-dye aggregation processes which inhibit intercalation. The net effect will thus be a delicate compromise of these two opposite trends.

In particular, we have explored here the binding of tetrapyridyl d^8 metal complexes to RNA substrates, which are less studied with respect to their DNA analogues. Interestingly, the analysed metal complexes seem to react better with RNAs with respect to DNA, even in the triplex form. Indeed, the K_{app}(RNA)/K_{app}(DNA) ratio, in the case of double stranded poly(rA)poly(rU), ranges from 2.4 to 8.5 being $[Pd(H_2L2)]^{2+}$ > $[Pd(H_2L1)]^{2+}$ > $[Pd(L3)]^{2+}$ > $[Au(L1)]^{+}$. For triple stranded poly(rA)poly(rU) the same K_{app}(RNA)/K_{app}(DNA) ratio goes from 2.5 to 15 being $[Pd(L3)]^{2+}$ > $[Pd(H_2L2)]^{2+}$ > $[Au(L1)]^{+}$ >> $[Pd(H_2L1)]^{2+}$.

The more hindered/distorted $[Pd(H_2L2)]^{2+}$ species, which undergoes partial intercalation only, does not distinguish much poly(rA)poly(rU) from poly(rA)2poly(rU). Interestingly, all species are also able to strongly stabilise complex structures as poly(rA)2poly(rU) triple helices with a ΔT_m in the 10 - 20 °C range.

As for the binding with the RNA-4WJ, $[Pd(H_2L1)]^{2+}$ and $[Au(L1)]^{+}$ metal complexes seem to be species able to bind RNA at the junction. In fact, they show binding features which appear only in the presence of RNA-4WJ and not for its x-r strands RNA duplex counterpart. These species, similarly to $Pt(H_2L1)]^{2+}$/DNA-4WJ structure,[22] may possess those specific molecular properties which trigger/stabilise a peculiar superstructure. Further studies are ongoing to elucidate this point.

Author Contributions

Conceptualisation: C.G., L.M., S.B., A.P., T.B.; data curation: F.B., D.C.; formal analysis: F.B, C.E., D.C.; funding acquisition: C.G., L.M., S.B., A.P., T.B.; investigation F.B., C.E., D.C., C. vdG. X-Q. Z.; methodology: D.C., A.P, T.B.; supervision: A.P., T.B.; writing-original draft: F.B.; writing-review and editing: all authors.

Conflicts of interest

There are no conflicts to declare.

Acknowledgements

We thank CIRCMSB (Consorzio Inter-Universitario di Ricerca in

Chimica dei Metalli nei Sistemi Biologici). This contribution is part of the work from COST Action CA18202, NECTAR Network for Equilibria and Chemical Thermodynamics Advanced Research, supported by COST (European Cooperation in Science and Technology).

References

1. B. W. Harper, F. Li, R. Beard, K. B. Garbutcheon-Singh, N. S. Ng and J. R. Aldrich-Wright, in *Supramolecular Systems in Biomedical Fields*, The Royal Society of Chemistry, 2013, DOI: 10.1039/9781849737821-00260, pp. 260-299.
2. F. Guarra, A. Pratesi, C. Gabbiani and T. Biver, *Journal of Inorganic Biochemistry*, 2021, **217**, 111355.
3. J. J. Criado, J. L. Manzano and E. Rodríguez-Fernández, *Journal of Inorganic Biochemistry*, 2003, **96**, 311-320.
4. B. Bertrand, M. R. M. Williams and M. Bochmann, *Chemistry – A European Journal*, 2018, **24**.
5. S. Ray, R. Mohan, J. K. Singh, M. K. Samantaray, M. M. Shaikh, D. Panda and P. Ghosh, *Journal of the American Chemical Society*, 2007, **129**, 15042-15053.
6. M. Heydari, M. E. Moghadam, A. Tarlani and H. Farhangian, *Applied Biochemistry and Biotechnology*, 2017, **182**, 110-127.
7. A. S. Abu-Surrah, *Cancer Therapy*, 2008, **6**, 1-10.
8. N. J. Patel, B. S. Bhatt and M. N. Patel, *Inorganica Chimica Acta*, 2019, **498**, 119130.
9. M. Pérez-Cabré, G. Cervantes, V. Moreno, M. J. Prieto, J. M. Pérez, M. Font-Bardia and X. Solans, *Journal of Inorganic Biochemistry*, 2004, **98**, 510-521.
10. E.-J. Gao, S.-M. Zhao, D. Zhang and Q.-T. Liu, *Chinese Journal of Chemistry*, 2005, **23**, 54-57.
11. E. Gao, M. Zhu, H. Yin, L. Liu, Q. Wu and Y. Sun, *Journal of Inorganic Biochemistry*, 2008, **102**, 1958-1964.
12. E.-J. Gao, K.-H. Wang, X.-F. Gu, Y. Yu, Y.-G. Sun, W.-Z. Zhang, H.-X. Yin, Q. Wu, M.-C. Zhu and X.-M. Yan, *Journal of Inorganic Biochemistry*, 2007, **101**, 1404-1409.
13. A. Shanmugapriya, R. Jain, D. Sabarinathan, G. Kalaiarasi, F. Dallemer and R. Prabhakaran, *New Journal of Chemistry*, 2017, **41**, 10324-10338.
14. E. Largy, F. Hamon, F. Rosu, V. Gabelica, E. De Pauw, A. Guédin, J.-L. Mergny and M.-P. Teulade-Fichou, *Chemistry – A European Journal*, 2011, **17**, 13274-13283.
15. J. J. King, K. L. Irving, C. W. Evans, R. V. Chikhale, R. Becker, C. J. Morris, C. D. Peña Martinez, P. Schofield, D. Christ, L. H. Hurley, Z. A. E. Waller, K. S. Iyer and N. M. Smith, *Journal of the American Chemical Society*, 2020, **142**, 20600-20604.
16. J. Spiegel, S. Adhikari and S. Balasubramanian, *Trends in Chemistry*, 2020, **2**, 123-136.
17. B. Chu, D. Zhang and P. J. Paukstelis, *Nucleic Acids Research*, 2019, **47**, 11921-11930.
18. N. Bandyopadhyay, P. Basu, G. S. Kumar, B. Guhathakurta, P. Singh and J. P. Naskar, *Journal of Photochemistry and Photobiology B: Biology*, 2017, **173**, 560-570.
19. C. E. Miron, M. R. Colden Leung, E. I. Kennedy, O. Fleischel, M. A. Khorasani, N. Wu, J.-L. Mergny and A. Petitjean, *Chemistry – A European Journal*, 2018, **24**, 18718-18734.
20. S. A. Elsayed, H. E. Badr, A. di Biase and A. M. El-Hendawy, *Journal of Inorganic Biochemistry*, 2021, **223**, 111549.
21. S. Hohng, T. J. Wilson, E. Tan, R. M. Clegg, D. M. J. Lilley and T. Ha, *Journal of Molecular Biology*, 2004, **336**, 69-79.
22. V. H. S. van Rixel, A. Busemann, M. F. Wissingh, S. L. Hopkins, B. Siewert, C. van de Griend, M. A. Siegler, T. Marzo, F. Papi, M. Ferraroni, P. Gratteri, C. Bazzicalupi, L. Messori and S. Bonnet, *Angewandte Chemie International Edition*, 2019, **58**, 9378-9382.
23. X.-Q. Zhou, M. Xiao, V. Ramu, J. Hilgendorf, X. Li, P. Papadopoulou, M. A. Siegler, A. Kros, W. Sun and S. Bonnet, *Journal of the American Chemical Society*, 2020, **142**, 10383-10399.
24. M. Hayashi and Y. Harada, *Nucleic Acids Research*, 2007, **35**, e125-e125.
25. Y. Babayan, G. Manzini, L. E. Xodo and F. Quadrifoglio, *Nucleic Acids Research*, 1987, **15**, 5803-5812.
26. A. Biancardi, T. Biver, A. Marini, B. Mennucci and F. Secco, *Physical Chemistry Chemical Physics*, 2011, **13**, 12595-12602.
27. P. Klimkowski, S. De Ornellas, D. Singleton, A. H. El-Sagheer and T. Brown, *Organic & Biomolecular Chemistry*, 2019, **17**, 5943-5950.
28. C. Pérez-Arnaiz, N. Busto, J. Santolaya, J. M. Leal, G. Barone and B. García, *Biochimica et Biophysica Acta (BBA) - General Subjects*, 2018, **1862**, 522-531.
29. F. J. Hoyuelos, B. García, J. M. Leal, N. Busto, T. Biver, F. Secco and M. Venturini, *Physical Chemistry Chemical Physics*, 2014, **16**, 6012-6018.
30. T. Biver, F. Secco and M. Venturini, *Archives of Biochemistry and Biophysics*, 2005, **437**, 215-223.
31. B. Garcia, J. M. Leal, V. Paiotta, S. Ibeas, R. Ruiz, F. Secco and M. Venturini, *The Journal of Physical Chemistry B*, 2006, **110**, 16131-16138.
32. T. Biver, D. Lombardi, F. Secco, M. Rosaria Tiné, M. Venturini, A. Bencini, A. Bianchi and B. Valtancoli, *Dalton Transactions*, 2006, DOI: 10.1039/B512820J, 1524-1533.
33. F. Secco, M. Venturini, T. Biver, F. Sánchez, R. Prado-Gotor and E. Grueso, *The Journal of Physical Chemistry B*, 2010, **114**, 4686-4691.
34. D. R. Duckett, A. I. H. Murchie and D. M. J. Lilley, *Cell*, 1995, **83**, 1027-1036.
35. M. E. Fornace, N. J. Porubsky and N. A. Pierce, *ACS Synthetic Biology*, 2020, **9**, 2665-2678.
36. F. Macii, C. Perez-Arnaiz, L. Arrico, N. Busto, B. Garcia and T. Biver, *Journal of Inorganic Biochemistry*, 2020, **212**, 111199.
37. N. Busto, D. C. Romero, A. Revilla-Cuesta, I. Abajo, J. V. Cuevas, T. Rodríguez, B. García and T. Torroba, *Dyes and Pigments*, 2022, **205**, 110557.
38. K. W. Lim, P. Alberti, A. Guédin, L. Lacroix, J.-F. Riou, N. J. Royle, J.-L. Mergny and A. T. Phan, *Nucleic Acids Research*, 2009, **37**, 6239-6248.
39. C. Bazzicalupi, M. Ferraroni, F. Papi, L. Massai, B. Bertrand, L. Messori, P. Gratteri and A. Casini, *Angewandte Chemie International Edition*, 2016, **55**, 4256-4259.
40. T. Biver, C. Cavazza, F. Secco and M. Venturini, *Journal of Inorganic Biochemistry*, 2007, **101**, 461-469.
41. L. S. Lerman, *Journal of Molecular Biology*, 1961, **3**, 18-IN14.

42. T. Šmidlehner, I. Piantanida and G. Pescitelli, *Beilstein Journal of Organic Chemistry*, 2018, **14**, 84-105.
43. A. Silvestri, G. Barone, G. Ruisi, D. Anselmo, S. Riela and V. T. Liveri, *Journal of Inorganic Biochemistry*, 2007, **101**, 841-848.
44. A. Casini, C. Gabbiani, E. Michelucci, G. Pieraccini, G. Moneti, P. J. Dyson and L. Messori, *JBIC Journal of Biological Inorganic Chemistry*, 2009, **14**, 761-770.
45. S. M. Meier, C. Gerner, B. K. Keppler, M. A. Cinellu and A. Casini, *Inorganic Chemistry*, 2016, **55**, 4248-4259.
46. S. J. Shields, O. Oyeyemi, F. C. Lightstone and R. Balhorn, *Journal of the American Society for Mass Spectrometry*, 2003, **14**, 460-470.
47. G. Chen, M. Fan, Y. Liu, B. Sun, M. Liu, J. Wu, N. Li and M. Guo.
48. C. Zoppi, L. Messori and A. Pratesi, *Dalton Transactions*, 2020, **49**, 5906-5913.
49. G. Tamasi, A. Carpini, D. Valensin, L. Messori, A. Pratesi, F. Scaletti, M. Jakupec, B. Keppler and R. Cini, *Polyhedron*, 2014, **81**, 227-237.
50. T. Urathamakul, D. J. Waller, J. L. Beck, J. R. Aldrich-Wright and S. F. Ralph, *Inorganic Chemistry*, 2008, **47**, 6621-6632.
51. C. Riccardi, D. Capasso, G. M. Rozza, C. Platella, D. Montesarchio, S. Di Gaetano, T. Marzo, A. Pratesi, L. Messori, G. N. Roviello and D. Musumeci, *Journal of Inorganic Biochemistry*, 2020, **203**, 110868.
52. P. Gratteri, L. Massai, E. Michelucci, R. Rigo, L. Messori, M. A. Cinellu, C. Musetti, C. Sissi and C. Bazzicalupi, *Dalton Transactions*, 2015, **44**, 3633-3639.
53. D. Ghosh, F. Rosu and V. Gabelica, *Analytical Chemistry*, 2022, **94**, 15386-15394.
54. E. Largy, A. König, A. Ghosh, D. Ghosh, S. Benabou, F. Rosu and V. Gabelica, *Chemical Reviews*, 2022, **122**, 7720-7839.
55. D. Bhattacharyya, G. Mirihana Arachchilage and S. Basu, *Frontiers in Chemistry*, 2016, **4**.
56. V. Gabelica, *Accounts of Chemical Research*, 2021, **54**, 3691-3699.
57. F. Guarra, T. Marzo, M. Ferraroni, F. Papi, C. Bazzicalupi, P. Gratteri, G. Pescitelli, L. Messori, T. Biver and C. Gabbiani, *Dalton Transactions*, 2018, **47**, 16132-16138.
58. G. W. Collie, G. N. Parkinson, S. Neidle, F. Rosu, E. De Pauw and V. Gabelica, *Journal of the American Chemical Society*, 2010, **132**, 9328-9334.
59. F. Rosu, V. Gabelica, H. Poncelet and E. De Pauw, *Nucleic Acids Research*, 2010, **38**, 5217-5225.
60. L. Massai, C. Zoppi, D. Cirri, A. Pratesi and L. Messori, *Frontiers in Chemistry*, **8**, 581648.
61. A. Pratesi, D. Cirri, D. Fregona, G. Ferraro, A. Giorgio, A. Merlino and L. Messori, *Inorganic Chemistry*, 2019, **58**, 10616-10619.
62. L. Messori, F. Scaletti, L. Massai, M. A. Cinellu, I. Russo Krauss, G. di Martino, A. Vergara, L. Paduano and A. Merlino, *Metallomics*, 2014, **6**, 233-236.
63. D. O. Ł. R.-Z. D. S. G. v. E. R. L.-T. o. t. S. o. P. C. w. C. Porębska, *Journal*, 2021, **22**.
64. T. Biver, A. Boggioni, F. Secco, E. Turriani, M. Venturini and S. Yarmoluk, *Archives of Biochemistry and Biophysics*, 2007, **465**, 90-100.
65. T. Biver, A. Boggioni, B. García, J. M. Leal, R. Ruiz, F. Secco and M. Venturini, *Nucleic Acids Research*, 2010, **38**, 1697-1710.